# A Virtual Impedance Enhancement Based Transformer-Less Active EMI Filter for Conducted EMI Suppression in Power Converters

Zhe Zhang, *Student Member, IEEE*, Ali M. Bazzi, *Senior Member, IEEE*

***Abstract*- Due to the successive switching actions in a power electronic system, considerable conducted electromagnetic interference (EMI) is generated. This has been a major concern in designing power converters, which requires additional EMI filtering efforts. Passive EMI filters are the most common solutions to EMI reduction but usually consume a large portion of the volume as well as weight in power converters. Active EMI filters (AEFs) or hybrid EMI filters (HEFs) are considered best candidates over traditional passive EMI filters to achieve higher power density in power converters. The utilization of current transformer to sense or to compensate the EMI noise can increase the volume of an AEF. In this paper, a transformer-less AEF, sprung from the concept of virtual impedance enhancement, is proposed. The proposed design features feedforward control with current-sensing-voltage-compensating. The operation principle of the proposed AEF is thoroughly introduced, and its performance is evaluated through simulations and experiments. Experimental results with an AC-DC power converter and a DC-AC inverter show that the proposed AEF can be generally applied to reduce conducted EMI on either AC or DC power lines.**

***Index Terms*- Active filter, electromagnetic interference (EMI), conducted emissions, virtual impedance enhancement, AC-DC converter, DC-AC inverter.**

## I. Introduction

The past few decades have seen extensive use of power electronic converters in clean and distributed energy sources, as well as energy storage systems, transportation systems, and the power grid. Pulse width modulation (PWM), the most prevalent technique to operate power converters, has enabled reduced size, weight, and operational costs of these converters while increasing the overall energy efficiency [1]. However, due to the rapid transients associated with the switching process of the power semiconductors, i.e. high *dv/dt* and/or *di/dt*, electromagnetic interference (EMI) problem will arise. The generated noise currents propagate along the input and output power lines via parasitic capacitance and would, in turn, cause interference with ambient electronic systems [2], [3].

EMI can be in the form of either radiated emission or conducted emission depending on the frequency of concern [4]. Different EMI regulations were set forth to limit the conducted EMI from the power electronic circuits [2], [5]. The frequency range as well as the maximum permissible magnitude of conducted EMI are defined within these standards. Most endeavors by researchers have been focused on understanding and effectively suppressing conduced EMI. Fig. 1 summarizes all research topics relevant to conducted EMI. The research of conducted EMI can be categorized into three different aspects: EMI characterization, EMI modeling, and EMI mitigation [6].

This paper mainly discusses EMI mitigation. To combat the adverse effect induced by conducted EMI, mitigation approaches can be taken either at source or along the propagation path. Effectively managing conducted EMI at the source, namely the power converter side, reduces filtering needs to attenuate EMI. Random switching frequency PWM, deemed as a promising technique to suppress conducted EMI, is reportedly applied in adjustable speed drives (ASD) [7]-[10]. Balanced or improved inverter topologies have been developed to achieve better common mode voltage (CMV) performance for motor drives [11]-[14]. Active gate drive methods are proposed aiming at limiting *dv/dt* transient of a power semiconductor and suppressing the concurrent ringing associated with the switching action [15], [16]. All these references show attempts to mitigate conducted EMI at its source.

The most common and practical solutions to conducted EMI suppression is installing passive EMI filters since it is unrealistic to expect a noise-free power converter on its own. The typical configuration of a passive EMI filter that constitutes big inductors and capacitors is shown in Fig. 2. Since inductors must carry the full load current and the capacitors have to withstand high voltages, passive EMI filters are usually bulky and heavy. In some applications, the passive EMI filters can take up more than 30% of the total volume in a power converter [17]. Various studies are carried out to systematically design passive EMI filters with optimized volume as well as conducted emission attenuation for different power converters [18]-[20], [40]-[46]. Hybrid filters which incorporate active and smaller passive filters have the potential to reduce the volume of the filter by up to 58% [21]. The active filter is mainly responsible for suppressing the EMI in the low-frequency range and, consequently, the corner frequency of the passive filter can be increased, which allows for immediate volume reduction of a passive filter.

The full potential of active EMI filters (AEFs) is receiving significant research interest. The technique of active filtering was first introduced in [22], which later gave rise to the modeling and design of emerging active EMI filters [23]-[31]. In [24], a common-mode (CM) voltage cancellation circuit that utilizes complementary transistors and CM voltage transformer

Fig. 1. Research areas in conducted EMI.

Fig. 2. Typical configuration of a passive EMI filter: (a) schematic; (b) prototype.

at the output terminal of an induction motor drive to inject opposite CM voltage is proposed. The active cancellation circuit is reportedly able to reduce CM voltage by 250 V in an inverter-fed induction motor system switching at 5 kHz. A system model of a differential-mode (DM) AEF for AC/DC power converters is developed in [25]. The DM AEF relies on a current transformer for current sensing, and the stability of the filter as well as its compensation are discussed to guarantee good EMI reduction. The measured effective insertion gain of the DM AEF in the frequency range of 100 kHz-10 MHz has achieved a maximum of -20 dB. A study and practical implementation of an active filter based on high-frequency (HF) power amplifier is carried out in [26]. The proposed active filter along with additional chokes is tested with a three-phase 6.8 kVA power converter and produces effective attenuation up to 50 kHz with ~10 dBμV reduction at maximum. Chen et al. propose an active circuit that can boost the impedance of an inductor to a great extent and apply it in PWM ASD system [27]. The proposed filter is reported to be able to reduce the peak-to-peak value of CM voltage by 68%-80% within the drive's operation frequency range. These designs, to a great extent, rely on magnetic components such as transformers or chokes to achieve better performance. In [28], a transformer-less AEF is designed to suppress DC-side CM EMI in motor drive system. The CM impedance of the motor must be characterized first and artificially synthesized by a scaled impedance network for the AEF to function properly. However, it is difficult to achieve perfect scaled synthesis of the motor's CM impedance, and the transformer-less AEF in [28] is reported to achieve conducted EMI attenuation up to 10 MHz with a maximum reduction of ~15 dBμA.

Apart from those analog solutions mentioned above, researchers have also explored the possibility of EMI reduction using digital approach [32]-[34]. An FPGA based digital AEF is proposed in [32] with the application in photovoltaic microinverter. With high-speed analog-to-digital converter (ADC), the conducted noise is digitized and inverted through the digital controller-FPGA. Then the digitally inverted signal is reconstructed and injected back electrically with digital-to-analog converter (DAC). In [33], the delay time of digital processing for the AEF is considered and compensated to improve the performance of digital AEF in an arc welding inverter. Peng et al. further combine the digital AEF with proportional resonant controller to provide high gain at frequencies of interest [34]. The combined control scheme for the AEF is reported to improve the EMI attenuation in a buck converter by another 20 dB. The digital solutions are quite computationally intensive and are not cost-effective due to the use of expensive digital platforms.

However, very few literatures have discussed the viability of designing a transformer-less current-sensing-voltage-compensating AEF. In this paper, the concept of virtual impedance enhancement is explored and applied in the context of designing an AEF. Such concept is extremely helpful in enabling the design of a transformer-less current-sensing-voltage-compensating AEF. The paper is organized as follows. Section II firstly reviews the basics of active EMI filter. Section III then discusses the modeling of conducted EMI in power

converters. Modeling and design of the proposed AEF based on the concept of virtual impedance enhancement is presented in detail in Section IV. Simulation and experimental results are included in Section V to demonstrate the effectiveness of the proposed AEF. Section VI concludes the paper.

## II. Basics of Active EMI Filter

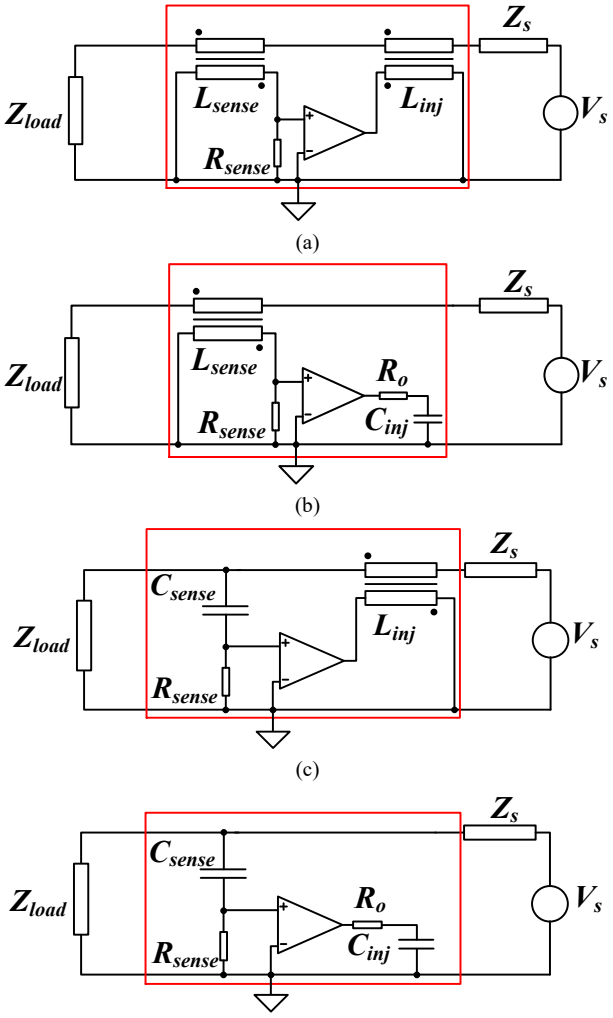


Fig. 3. Four types of active filtering circuits: (a) current-sensing-voltage-compensating (CSVC); (b) current-sensing-current-compensating (CSCC); (c) voltage-sensing-voltage-compensating (VSVC); (d) voltage-sensing-current-compensating (VSCC).

In general, the operation principles of an AEF are twofold: the first aspect is sensing the EMI noise present in the system and the second is compensating for the conducted EMI noise as much as possible. Four major types of active filtering circuits are summarized and shown in Fig. 3 based on the type of signals being sensed and compensated.

According to the literatures, the noise current can be sensed via current transformer and compensated through capacitor, while the noise voltage can be sensed via capacitor and compensated through transformer. The compensation relies on reverse injection for noise cancellation.

## III. Conducted EMI Modeling In Power Converters

In power electronic systems, the semiconductors, either discrete components or power modules, serve as the fundamental building blocks. These devices which are frequently switching in a power converter can be identified as the culprit of conducted EMI. Drastic fluctuation of voltage potential, associated with the device's switching action, results in significant conducted EMI throughout the system. Fig. 4 shows an example of the conducted EMI measurement for a commercial 100-240 VAC to 5 VDC power adaptor. The conducted EMI spectrum of a power converter can be generally divided into two regions in terms of major contributing factor: low-frequency (150 kHz to several MHz) and high-frequency (several MHz to 30 MHz) region. The low-frequency region is dominated by the pulsed voltage sequence, while the high-frequency region is predominantly influenced by each pulse's rising/falling transients as there are a great number of superimposed oscillations at higher frequencies.

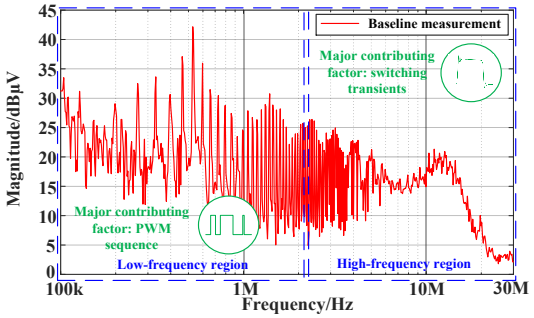


Fig. 4. Conducted EMI measurement for a 1.5W AC-DC converter.

To model the effect of conducted EMI, the single device or bridge module can be considered as a voltage source based on substitution theorem [35]. Fig. 5 illustrates replacing the single device/bridge module with voltage source and parasitic inductance/capacitance to develop an equivalent circuit for conducted EMI modeling. Following the same approach, one can easily derive either a Thevenin equivalence or a Norton equivalence by lumping all substituted voltage source in any converter topology.

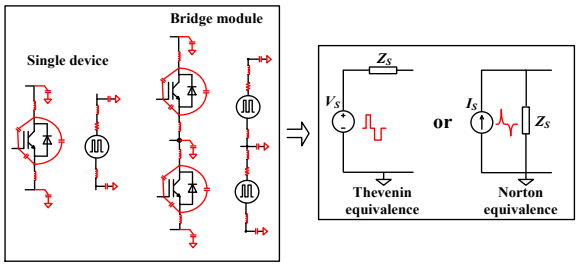


Fig. 5. Noise source modeling: Thevenin equivalence/Norton equivalence.

Typical measurement of conducted EMI often requires the separation of the noise source and its victim. A line impedance stability network (LISN), shown in Fig. 6, would be placed between the equipment under test (EUT) and power supply. The reason of using LISN is to achieve reproducible measurements and to decouple the power source's impact on EUT [36]. A general Norton equivalent model for conducted EMI

measurement in a power converter can be obtained as shown in Fig. 7. $Z_s(s)$, $Z_{line}(s)$ and $Z_{LISN}(s)$ represent the noise source impedance, line impedance and LISN's impedance, respectively. DM and CM noise are not differentiated since they presume similar characteristics except for their circulation path. The open-loop gain $G_{OL}(s)$ is defined as:

$$G_{OL}(s) = I_O / I_S = \frac{Z_S(s)}{Z_S(s) + Z_{LISN}(s) + Z_{line}(s)} \quad (1)$$

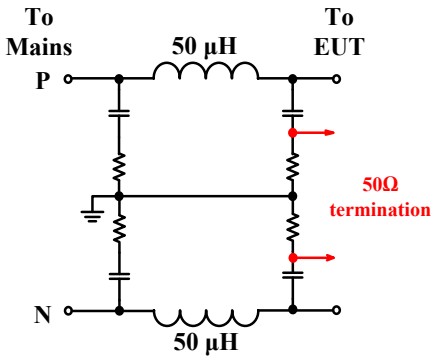


Fig. 6. Schematic of a single-phase line impedance stability network (LISN).

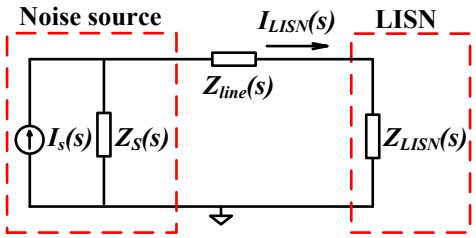


Fig. 7. General equivalent model for conducted EMI measurement in a power converter.

## IV. Modeling And Design Of The Proposed AEF

Instead of adopting the framework of noise cancellation by reverse injection, the design of an AEF can be envisioned from a different perspective: that is actively controlling a device to make it possess the characteristic similar to a passive filtering component which, in this case, a capacitor. The development of the proposed AEF based on the concept of virtual impedance enhancement will be elaborated on afterward.

There is no fundamental difference between CM and DM AEF in terms of their operation principles. The concept of virtual impedance enhancement can be generally applied in designing either DM or CM AEF depending on what type of noise signal is being sensed and compensated.

### *A. Virtual Impedance Enhancement (VIE)*

It is generally known that a capacitor is a passive device whose voltage across the two terminals and conducting current should satisfy equations (2) and (3) where $C$ is the capacitance. In another sense, a capacitor can be considered as a current controlled voltage source (CCVS). The controlled voltage source's output $v_s$ is dependent on the flowing-through current $i_s$. Such relationship can be summarized as equation (4) in time-domain. The integral gain $k$ can be analogous to the reciprocal of the effective capacitance.

$$v_c = Z(s) i_c \quad (2)$$

$$Z(s) = 1/sC \quad (3)$$

$$v_s = k\int i_s dt \qquad k = 1/C_{eff} \quad (4)$$

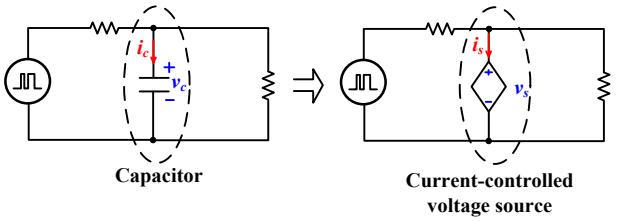


Fig. 8. Illustration of virtual impedance enhancement: a virtual capacitor realization.

The principle of virtual impedance enhancement (VIE), inspired by the characteristics of a capacitor mentioned above [37], is illustrated in Fig. 8. Suppose that an emulated voltage source is created such that its output voltage is subject to equation (4). The variable $i_s$ now being integrated is the high-frequency noise current present in the line. Therefore, such controlled voltage source exactly shows a capacitor's behavior so that the high-frequency noise current is steered by the controlled voltage source due to its capacitive characteristic. According to equation (4), the effective capacitance $C_{eff}$ by the emulated voltage source can be actively manipulated by tuning the integral gain. Such concept of virtual impedance enhancement leads to a virtual capacitor realization, which is extremely appealing and will be applied in designing general-purpose current-sensing-voltage-compensating AEF.

### *B. System Modeling of The Proposed VIE Based AEF*

Current sensing is preferred over voltage sensing because the emulated voltage source shown in Fig. 8 relies on the noise current to perform virtual capacitor realization. A high-pass filter (HPF) would be needed to reject the fundamental or DC component in the sensed current depending on whether the AEF is adopted at AC-side or DC-side in the system.

Two possible control schemes: feedback and feedforward control can be applied in designing an AEF. Fig. 9 (a) shows an equivalent circuit of the proposed AEF with feedback control and Fig. 9 (b) shows an equivalent circuit of feedforward-controlled AEF. $Z_o(s)$ is the output impedance of the emulated voltage source and $Z_{dec}(s)$ is the impedance of any decoupling network. The feedback and feedforward controllers are denoted as $G_{fb}(s)$ and $G_{ff}(s)$, respectively:

$$G_{fb}(s) = k_{fb} G_{1st\_HPF}(s) G_{int}(s) \quad (5)$$

$$G_{ff}(s) = k_{ff} G_{1st\_HPF}(s) G_{int}(s) \quad (6)$$

$$G_{1st\_HPF}(s) = Ts/(1+Ts) \quad (7)$$

$$G_{int}(s) = 1/s \quad (8)$$

where $k_{fb}$ and $k_{ff}$ represent feedback and feedforward gains of the controller, respectively, $G_{1st\_HPF}(s)$ represents the transfer

function of a first-order high-pass filter (HPF), $T$ is the time constant for the HPF, and $G_{int}(s)$ represents the transfer function of an integrator which assumes the role of virtual impedance enhancement.

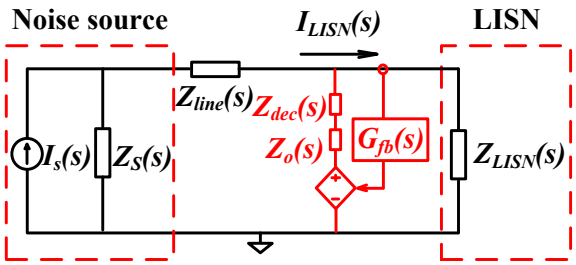


(a)

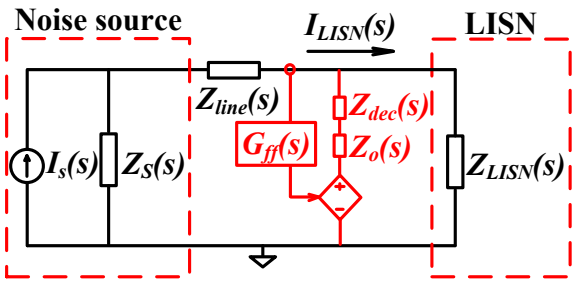


(b)

Fig. 9. Equivalent model for proposed AEF: (a) feedback control with Norton equivalence; (b) feedforward control with Norton equivalence.

To evaluate the performance of a filter, the term insertion loss ($IL$) is usually used and defined in equation (9). The signal flow diagrams for proposed feedback-controlled and feedforward-controlled AEF are shown in Fig. 10 (a) and (b), respectively. The diagrams can be further reduced into simplified feedback systems shown in Fig. 11, which makes it more convenient to derive the corresponding insertion loss for the proposed AEF.

$$IL = I_{LISN} / I_s \tag{9}$$

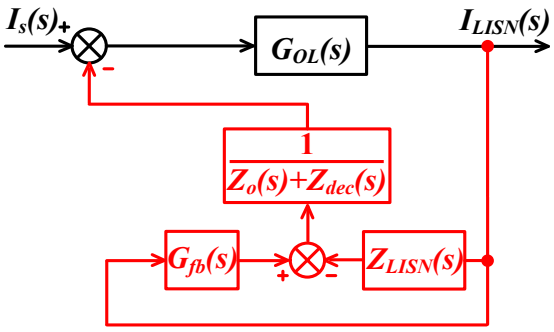


(a)

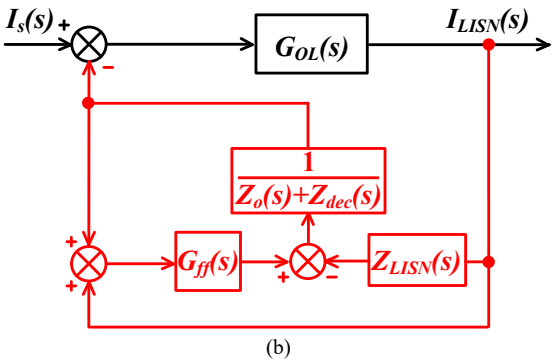


(b)

Fig. 10. Signal flow diagram of proposed AEF: (a) feedback control; (b) feedforward control.

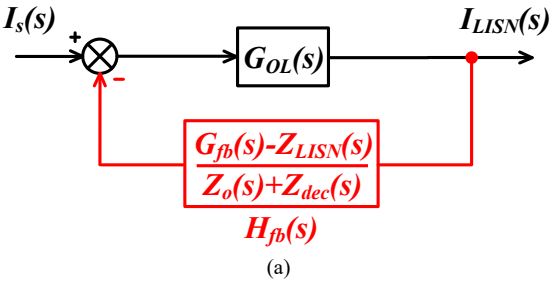


(a)

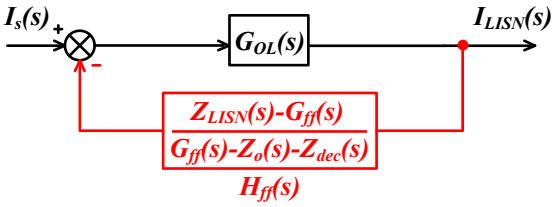


(b)

Fig. 11. Reduced and simplified signal flow diagram of proposed AEF: (a) feedback control; (b) feedforward control.

The equations for insertion loss of the proposed feedback- and feedforward-controlled AEF are derived as follows:

$$H_{fb}(s) = \frac{G_{fb}(s) - Z_{LISN}(s)}{Z_o(s) + Z_{dec}(s)} \tag{10}$$

$$H_{ff}(s) = \frac{Z_{LISN}(s) - G_{ff}(s)}{G_{ff}(s) - (Z_o(s) + Z_{dec}(s))} \tag{11}$$

$$IL_{fb} = \frac{G_{OL}(s)}{1 + G_{OL}(s) * H_{fb}(s)} \tag{12}$$

$$IL_{ff} = \frac{G_{OL}(s)}{1 + G_{OL}(s) * H_{ff}(s)} \tag{13}$$

Ideally, $I_{LISN}$ is expected to diminish as much as possible to make the most of a filter. That means the insertion loss should approach zero for the proposed feedback- and feedforward-controlled AEF. To achieve such condition, by analyzing equations (5)-(13), an excessively large open-loop gain is preferred, yield:

$$G_{OL}(s) * H_{fb}(s) \to \infty \tag{14}$$

$$G_{OL}(s) * H_{ff}(s) \to \infty \tag{15}$$

Since the open-loop gain $G_{OL}(s)$ previously defined in (1) has not been influenced by the controller, it could be considered as constant for insertion loss analysis. This will consequently lead to the requirement that $H_{fb}(s)$ and $H_{ff}(s)$ be maximized so as to minimize the insertion loss. By examining (10) and (11), the following conditions given in (16) and (17) should be met accordingly:

$$G_{fb}(s) \to \infty \tag{16}$$

$$G_{ff}(s) / (Z_o(s) + Z_{dec}(s)) \approx 1 \tag{17}$$

For a feedback-controlled AEF, it is required that the controller's gain be extremely large or close to infinity based on the above analysis. However, there is a potential risk that the extremely large gain can cause the closed-loop system to become unstable.

For a feedforward-controlled AEF, if the output impedance of the controlled voltage source $Z_o(s)$ is negligible, it is required that the gain and phase provided by the controller match the impedance of decoupling network to achieve good insertion loss. In this sense, the feedforward control scheme, due to its requirement of bounded gain, is preferred over the feedback control scheme in designing the VIE based AEF. In the following section, detailed realization of the propose VIE based transformer-less AEF will be discussed.

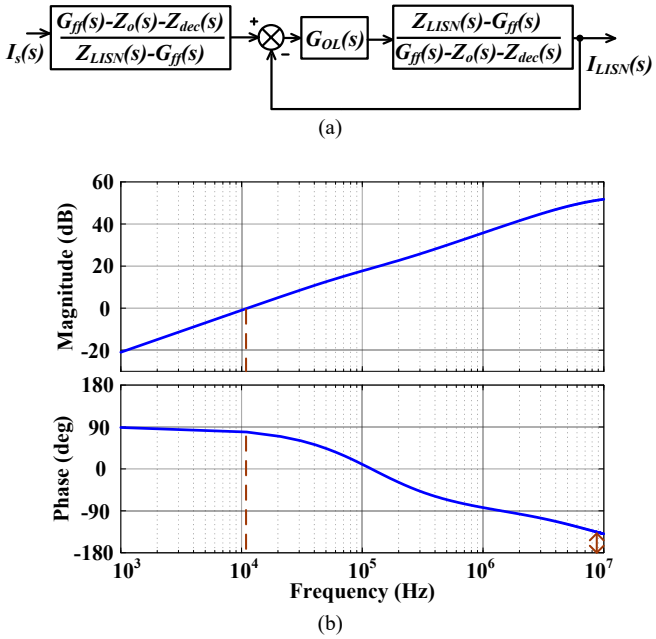


Fig. 12. Stability analysis of the proposed AEF: (a) block diagram; (b) Bode plot.

Stability analysis is critical with regard to AEF design [47]-[49], and the stability analysis model of the proposed AEF is developed and shown in Fig. 12 (a). The loop gain $G_L(s)$ is derived as:

$$G_L(s) = \frac{Z_s(s)[Z_{LISN}(s) - G_{ff}(s)]}{[Z_s(s) + Z_{LISN}(s) + Z_{line}(s)][G_{ff}(s) - Z_{dec}(s)]} \tag{18}$$

Based on $G_L(s)$, the Bode plot is shown in Fig. 12 (b). $G_L(s)$ crosses the 0-dB axis at approximately 11 kHz with a phase margin more than 90° and assumes an infinite gain margin within the frequency range of interest.

### *C. Design of VIE Based Transformer-less Feedforward-controlled AEF*

Current transformers have been reportedly used for current sensing in designing AEFs in other literatures [25], [38]. The parasitic output inductance and capacitance of a CT will form a resonant tank at certain high frequency, which might cause instability issue in the current sensing circuit. Moreover, CT based current sensing scheme can only be applied in AC and the use of ferrite magnetic core would, to a certain extent, add up to the filter's volume.

To achieve a more compact and transformer-less design of an AEF, the shunt resistor current sensing scheme is preferred due to its simplicity and general applicability. Such method is widely used in the application of power factor correction and over-current protection. Fig. 13 illustrates an example of shunt resistor current sensing circuit based on op-amp difference amplifier. Any flowing-through current will present voltage drop across the shunt resister $R_{sense}$ and such voltage drop will be amplified by the gain set by the resistive network. Note that $R_{sense}$ should be much less than $R_1$ and $R_2$ in order to minimize resistive load effect. A first-order HPF to suppress the fundamental or DC component in the sensed signal is realized by a simple RC circuit shown in Fig. 14. The cut-off frequency $\omega_{c\_HPF}$ is given in equation (19).

$$V_{out} = (V_1 - V_2)\frac{R_2}{R_1} \quad R_1 = R_1^*, R_2 = R_2^* \tag{19}$$

$$\omega_{C\_HPF} = \frac{1}{RC} \tag{20}$$

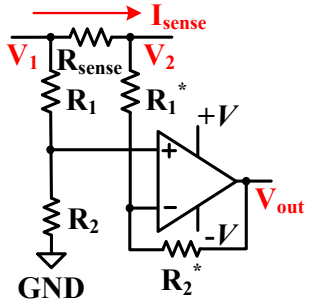


Fig. 13. Shunt resistor current sensing circuit.

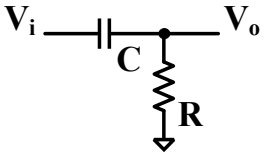


Fig. 14. First-order RC high-pass filter circuit.

The proposed AEF relies on integration of the sensed noise current as its voltage output to function as a virtual capacitor per the principle of virtual impedance enhancement. Fig. 15 (a) shows an integrator circuit with the aid of an op-amp, whose integral gain is set by 1/RC. Fig. 15 (b) shows the equivalent circuit of the op-amp based integrator. $R_{idm}$ and $C_{idm}$ represent

the op-amp's input impedance; $V_{OP}$ and $R_o$ represent the op-amp's output voltage and output impedance, respectively.

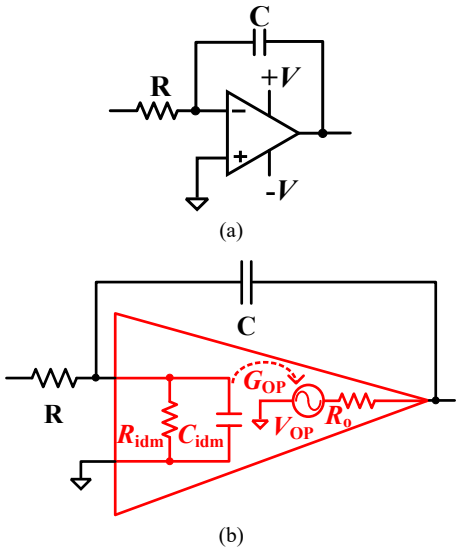


Fig. 15. Operational integrator: (a) Op-amp based integrator;(b) Equivalent circuit of the integrator.

To ensure the operational integrator's performance at higher frequencies, two main parameters of the op-amp in use should be paid careful attention to. The frequency of concern in the conducted EMI noise ranges from tens of kHz to several MHz, which poses a great challenge to the op-amp's gain bandwidth product. The open-loop gain of an op-amp is ideally infinite at all frequencies, but it is finite and dependent on frequency in reality. Fig. 16 illustrates the open-loop gain of a realistic op-amp, where the gain at low frequency is maximum and decreases linearly along with frequency. There is a point where the open-loop gain crosses the 0 dB line ($G_{OP}$ equal to 1). The frequency at which the open-loop gain reaches one is referred to as the unity gain bandwidth or gain bandwidth product (GBW). It is desired that GBW be as large as possible to cover frequency of concern in the conducted EMI when selecting the appropriate op-amp for operational integrator implementation.

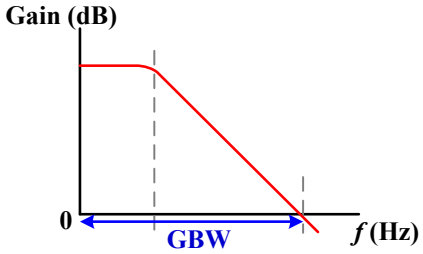


Fig.16. Realistic op-amp's open-loop gain vs. frequency.

Another important parameter in selecting the appropriate op-amp is the slew rate (SR). This parameter determines the fastest rate of change the op-amp's output can handle. For example, the maximum rate of change occurs at zero crossing in a sinusoidal signal and can be derived as:

$$R_m = 2\pi V_{\max} f \tag{20}$$

Fig. 17. Proposed design of transformer-less feedforward-controlled AEF.

where $R_m$ is defined as the maximum rate of change in a sinusoidal signal, $V_{max}$ is the maximum amplitude of a sinusoidal signal, and $f$ is the frequency of a sinusoidal signal. To be capable of reflecting on the sinusoidal signal promptly, the SR of an op-amp in use must satisfy:

$$\mathrm{SR} > R_m = 2\pi V_{max} f \tag{22}$$

A reasonably large SR that can capture the sensed high-frequency noise is also desired for the operational integrator to perform the expected virtual impedance enhancement.

In summary, the proposed design of a transformer-less feedforward-controlled AEF is shown in Fig. 17. The op-amp based current sensing network followed by an RC HPF is supposed to provide a scaled measurement of the high-frequency current present in the lines. The operational integrator is responsible for performing the virtual impedance enhancement to realize the proposed AEF. An additional push-pull power amplification stage, as shown in Fig. 18, could be concatenated with the integrator circuit if more current sourcing/sinking is desired [39].

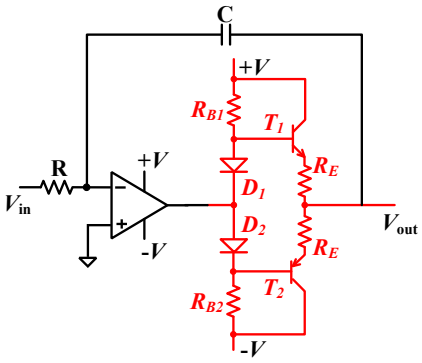


Fig. 18. Optional design of operational integrator with the capability of power amplification.

## V. Simulation And Experiment

### A. PSIM Simulation

A simplified circuit of the proposed AEF is built and simulated in PSIM for proof-of-concept. A square-wave voltage source to mimic the noise source as well as a single-phase LISN based on the model shown in Fig. 6 are used in the simulation. Fig. 19 shows the proof-of-concept simulation model. Dedicated blocks are available in PSIM to make the proposed feedforward-controlled AEF and the simulation parameters are summarized in TABLE I. The simulated conducted spectrum without and with the proposed AEF is shown in Fig. 20. Significant reduction in the conspicuous peaks is observed with the proposed AEF, which indicates the effectiveness of virtual impedance enhancement in designing an AEF.

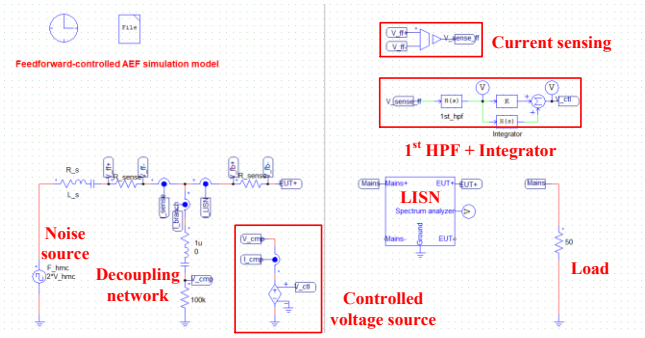


Fig. 19. Proof-of-concept simulation model in PSIM.

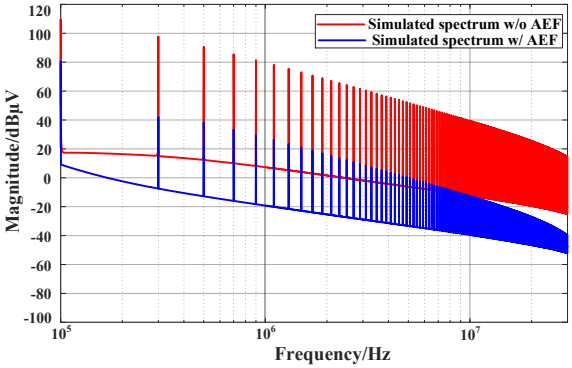


Fig. 20. Simulated conducted spectrum of proof-of-concept model (Red: without the proposed AEF; Blue: with the proposed AEF).

TABLE I
PARAMETERS OF SIMULATION MODEL

| | |
|---|---|
| Simulation timestep | 1E-8 s |
| Square-wave voltage source | 1 V pk-pk, 100 kHz |
| Decoupling network-capacitor | 1 μF |
| Decoupling network-resistor | 100 kΩ |
| Time constant for 1st HPF | 1E-5 s |
| Integral gain | 1E6 |

### B. Insertion Loss Evaluation

As discussed in previous section, the proposed feedforward-controlled AEF requires that its controller $G_{ff}(s)$ match the impedance of the decoupling network $Z_{dec}(s)$. This condition can be rewritten as:

$$G_{ff}(s) / Z_{dec}(s) \approx 1 \tag{23}$$

To assess how the feedforward controller $G_{ff}(s)$ deviating from the impedance of the decoupling network $Z_{dec}(s)$ will affect the stability of the proposed AEF, the stand-alone insertion loss of the proposed AEF is simulated with MATLAB. Fig. 21 illustrates the plot of the insertion loss of the proposed AEF dependent on $|G_{ff}(s)/Z_{dec}(s)|$. As can be seen, the best stand-alone insertion loss of the proposed AEF is achieved when $|G_{ff}(s)/Z_{dec}(s)|$ reaches 1, whereas the proposed AEF will be less effective beyond the match point.

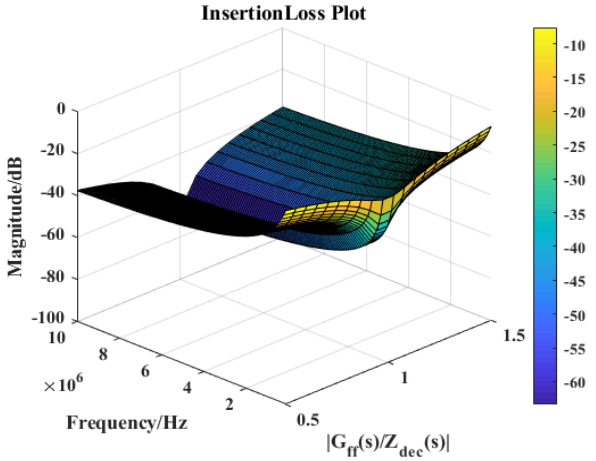


Fig. 21. Stand-alone insertion loss of the proposed AEF with dependency on $|G_{ff}(s)/Z_{dec}(s)|$.

Fig. 22 illustrates the design of the proposed transformer-less feedforward-controlled AEF. Most electronic components are surface mount devices (SMD) and no ferrite magnetic components are used, so the overall size of the AEF board can be made relatively small. TABLE II summarizes all the components used on the proposed AEF board. The prototype is first subjected to a vector network analyzer (VNA) for stand-alone insertion loss characterization. The measurement setup and measured stand-alone insertion loss of the AEF board are shown in Fig. 23 and Fig. 24, respectively. The VNA-Bode 100 performs a frequency sweep from 100 kHz to 30 MHz. More than 20 dB reduction is observed within the frequency range of 100 kHz-1 MHz, while 10 dB reduction on average is observed at frequencies beyond 1 MHz. It is unrealistic to guarantee a perfect match between $G_{ff}(s)$ and $Z_{dec}(s)$ at higher frequencies since the parasitic components (series inductance, leakage resistance, etc.) in the decoupling network become dominant, yielding completely different impedance characteristics of the decoupling network.

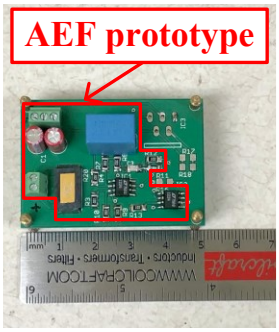


Fig. 22. Design of the proposed AEF board.

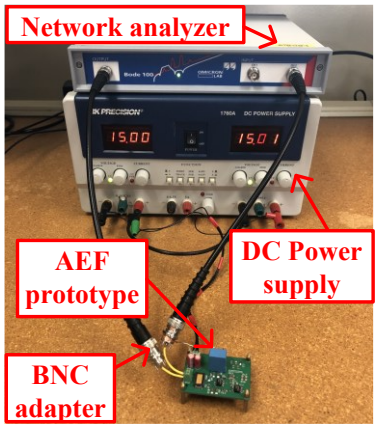


Fig. 23. Insertion loss measurement setup with Bode 100.

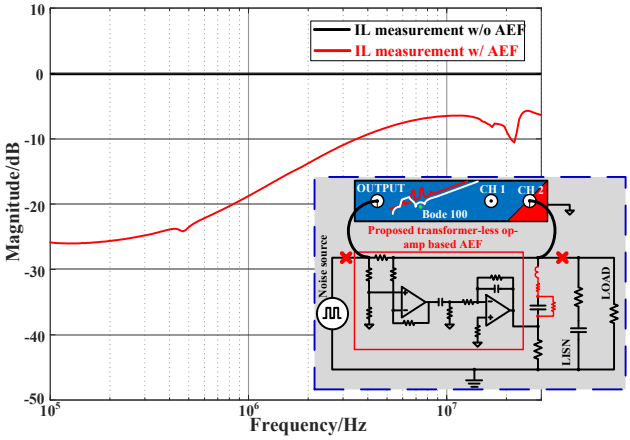


Fig. 24. Insertion loss characteristics of the proposed AEF board.

TABLE II
COMPONENTS IN THE PROPOSED AEF

| | |
|---|---|
| $R_{sense}$ | VISHAY DALE 0.25 Ω, 1% |
| $R_1$, $R_3$, $R_{int}$ | Panasonic Electronic Components 1 kΩ, 0.1% |
| $R_2$, $R_4$ | Panasonic Electronics Components 4 kΩ, 0.1% |
| $R_{limit}$ | Panasonic Electronic Components 100 kΩ, 0.1% |
| $C_{HPF}$, $C_{int}$ | Panasonic Electronics Components 1000 pF, 5% 100 VDC |
| $C_{dec}$ | EPCOS-TDK Electronics 1 µF, 10% 160 VAC |
| $U_1$, $U_2$ | Analog Devices Inc. LT1224, 45 MHz GBW |

*C. Experiments*

*1) Test with Function Generator*: The AEF prototype is first tested with a Tektronix function generator AFG3101 as emulated noise source. To mimic the operation of power converter, 50%-duty-cycle square-wave with amplitude of 100 mV at 100 kHz is generated from the function generator feeding standard 50 Ω resistive load. A 50 µH LISN-TBLC08 from TekBox along with spectrum analyzer-DSA815 from RIGOL is used for conducted emission measurement. The entire measurement setup is shown in Fig. 25 (a). Fig. 25 (b) shows the block diagram of this experimental setup. Fig. 26 shows the measured spectrum before and after applying the AEF prototype.

More than 20 dB reduction is achieved within 100 kHz-1 MHz. In addition, approximate 10 dB reduction is observed beyond 1 MHz. The designed AEF is showing consistent performance with regard to the stand-alone insertion loss characteristics.

*2) Test with AC-DC Converter*: The AEF prototype is further tested with a 7.5 W commercial power adaptor. The power adaptor is an AC-DC converter which converts 100-240 VAC to 5 VDC. The AEF is present at the power adaptor's input to suppress the conducted EMI from AC power lines. The entire measurement setup is shown in Fig. 27 (a). Fig. 27 (b) shows the block diagram of this experimental setup. Fig. 28 shows the measured spectrum before and after applying the AEF prototype. The designed AEF shows excellent performance in conducted EMI reduction at the AC power line for this commercial AC-DC converter.

*3) Test with DC-AC Inverter*: The AEF prototype is finally tested with a three-phase DC-AC inverter to evaluate its performance at DC side. The DC bus voltage of the inverter is 100 V and a Y-connected three-phase R-L (100 Ω, 0.2 mH) load is connected to the inverter's output. The inverter is switching at 10 kHz under space vector PWM. The AEF is placed on the DC side to evaluate its performance in suppressing conducted EMI for DC-AC inverter. The entire setup is shown in Fig. 29 (a). Fig. 29 (b) shows the block diagram of this experimental setup. Fig. 30 shows the measured spectrum before and after applying the AEF prototype. The designed AEF shows overall satisfactory performance in conducted EMI reduction on the DC power line of the DC-AC inverter.

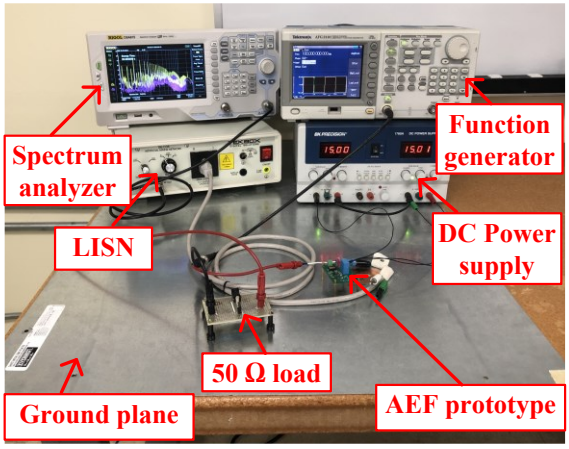


(a)

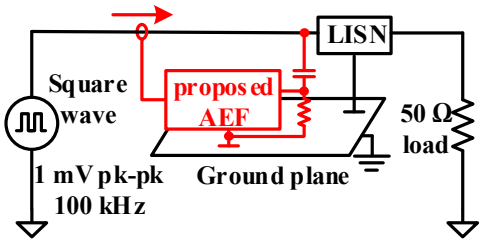


(b)

Fig. 25. Test with function generator: (a) measurement setup; (b) block diagram.

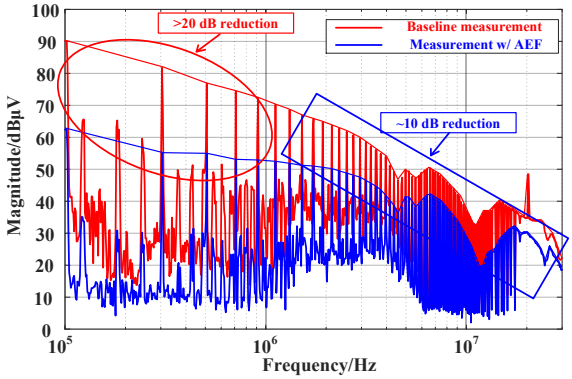


Fig. 26. Measured spectrum without/with the proposed AEF board.

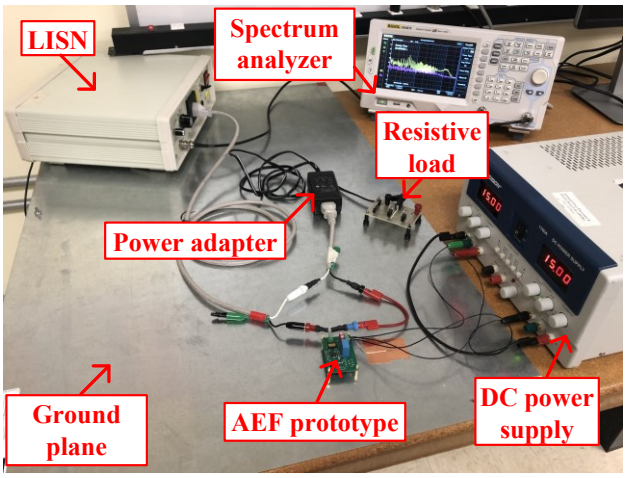


(a)

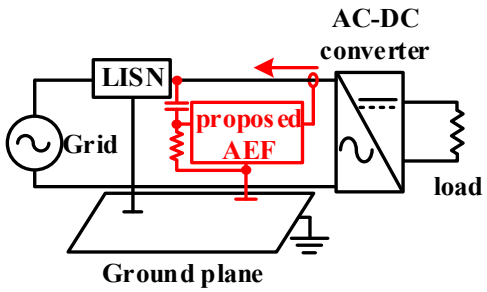


(b)

Fig. 27. Test with AC-DC converter: (a) measurement setup; (b) block diagram.

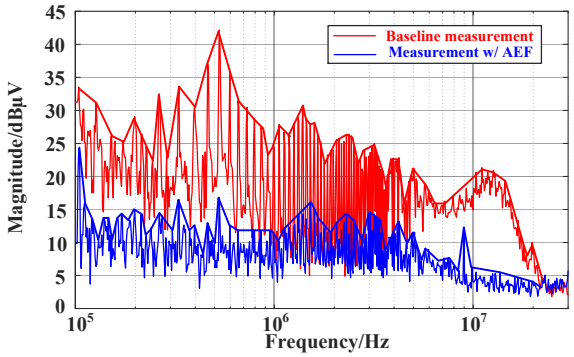


Fig. 28. Measured spectrum without/with the proposed AEF board.

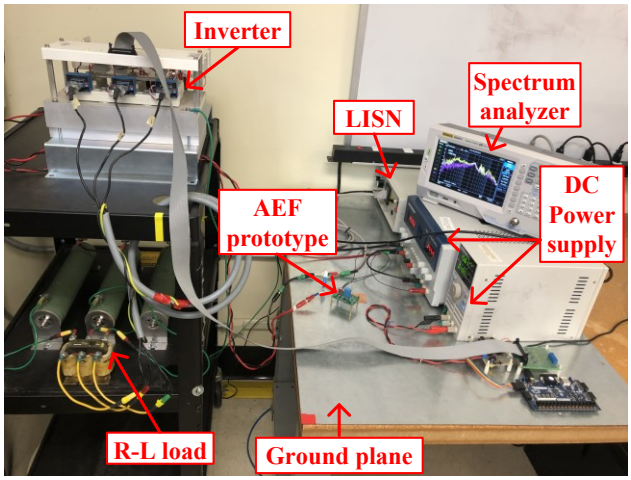


(a)

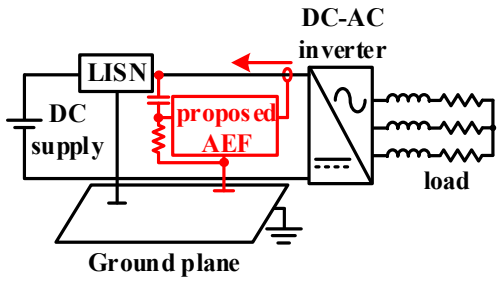


(b)

Fig. 29. Test with DC-AC inverter: (a) measurement setup; (b) block diagram.

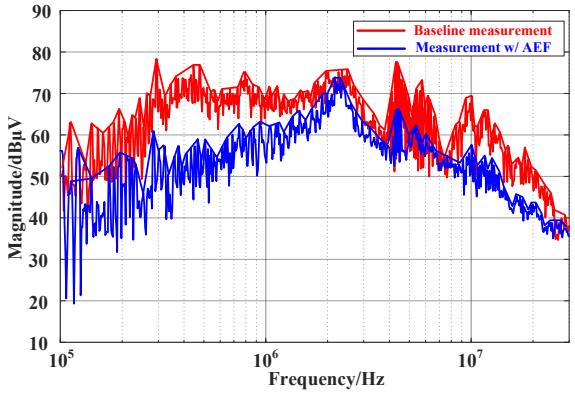


Fig. 30. Measured spectrum without/with the proposed AEF board.

*4) Discussion:* Note that the open-loop gain $G_{OL}(s)$ which is determined by the noise source characteristic $Z_s(s)$ will also affect the overall insertion loss of the system with AEF applied. Therefore, the final noise performance is a complex function of filter elements and noise source impedance, which vary in magnitude and phase over the frequency spectrum of interest [50]. The differences in achieved mitigations for AC-DC converter and DC-AC converter, compared to the measurement with a function generator are mainly due to their heterogeneous noise source characteristics. The noise source impedance of a function generator can be seen as standard 50 Ω over the frequency of interest, whereas the noise source impedance of AC-DC converter/DC-AC converter is highly non-linear.

## VI. Conclusions

In this paper, the concept of virtual impedance enhancement in the context of designing a transformer-less AEF for power converters is thoroughly discussed. Different from existing active filtering techniques which rely on reverse injection for noise cancellation, the proposed design features the realization of a virtual capacitor based on feedforward control of an op-amp based integrator. Simulation and experimental results have clearly validated the effectiveness of the proposed AEF. The proposed design can be potentially adopted at either AC-side or DC-side for conducted EMI suppression in power converters.

## Acknowledgment

This work was partially supported by National Science Foundation under Award 1752297.

## References

[1] D. Boroyevich, X. Zhang, H. Bishinoi, R. Burgos, P. Mattavelli, and F. Wang, "Conducted EMI and systems integration," in *8th International Conference on Integrated Power Systems (CIPS)*, 2014, pp. 1-14.

[2] K. Maninali, R. Oruganti, "Conducted EMI Mitigation Techniques for Switch-mode Power Converters: A Survey," *IEEE Trans. Power Electron.*, vol. 25, no. 9, pp. 2344-2356, Sept. 2010.

[3] H. Dai, T. M. Jahns, R. A. Torres, D. Han and B. Sarlioglu, "Comparative evaluation of conducted common-mode EMI in voltage-source and current-source inverters using wide-bandgap switches," *2018 IEEE Transportation Electrification Conference and Expo (ITEC)*, Long Beach, CA, 2018, pp. 788-794.

[4] H. W. Ott, "Noise reduction techniques" in *Electronic System*, Second Edition, John Wiley & Sons, 1988.

[5] C. R. Paul, *Introduction to Electromagnetic Compatibility.* 2nd ed. Hoboken, Neww Jersey, USA: Wiley, 2006.

[6] S. Cao *et al*., "Time–Frequency Characteristics Research of Common Mode Current in PWM Motor System," in *IEEE Transactions on Power Electronics*, vol. 35, no. 2, pp. 1450-1458, Feb. 2020.

[7] Z. Zhang, L. Wei, Y. Cui, P. S. Murthy and P. Yi, "Active EMI Reduction Technique of Active Front End (AFE) Drives Based on Randomized Switching Frequency PWM," *2019 IEEE Energy Conversion Congress and Exposition (ECCE)*, Baltimore, MD, USA, 2019, pp. 6438-6442.

[8] K. Lee, G. Shen, W. Yao, and Z. Lu, "Performance Characterization of Random Pulse Width Modulation Algorithms in Industrial and Commercial Adjustable-Speed Drives," *IEEE Trans. Ind. Appl.*, vol, 53, no. 2, March-April 2017.

[9] S. Bhattacharya, D. Mascarella, G. Joos, and G. Moschopoulos, "A Discrete Random PWM Technique for Acoustic Noise Reduction in Electric Traction Drives," *IEEE Energy Conversion Congress and Exposition (ECCE),* 2015, Montreal, QC, pp. 6811-6817.

[10] R. L. Kirlin, M. M. Bech, A. M. Trzynadlowski, "Analysis of Power and Power Spectral Density in PWM Inverters with Randomized Switching Frequency," *IEEE Trans. Ind. Electron*., vol. 49, no. 2, Apr. 2002.

[11] D. Han, C. T. Morris and B. Sarlioglu, "Common-Mode Voltage Cancellation in PWM Motor Drives with Balanced Inverter Topology," in *IEEE Transactions on Industrial Electronics*, vol. 64, no. 4, pp. 2683-2688, April 2017.

[12] C. T. Morris, D. Han and B. Sarlioglu, "Reduction of common-mode voltage and conducted EMI through three-phase inverter topology," *IEEE Trans. on Power Electron.*, vol. 32, no. 3, pp. 1720-1724, Mar. 2017.

[13] Z. Zhang, A. M. Bazzi and A. Semin, "An Active Zero-State Switch (AZS) for Commonmode Voltage Reduction in Voltage Source Inverter (VSI) Drives," *2020 IEEE Applied Power Electronics Conference and Exposition (APEC)*, New Orleans, LA, USA, 2020, pp. 711-717.

[14] H. Dai, R. A. Torres, J. Gossmann, W. Lee, T. M. Jahns and B. Sarlioglu, "An H7 Current-Source Inverter using Wide Bandgap Bidirectional Switches to Achieve High Efficiency and Low Conducted Common-Mode EMI," *2020 IEEE Applied Power Electronics Conference and Exposition (APEC)*, New Orleans, LA, USA, 2020, pp. 2519-2525.

[15] X. Yang, Y. Yuan, X. Zhang, and P. R. Palmer, "Shaping High-Power IGBT Switching Transitions by Active Voltage Control for Reduced EMI Generation," *IEEE Trans. Ind. Appl.*, vol. 51, no. 2, pp. 1669-1677, March-April 2015.

[16] S. Mahmodicherati, N. Ganesan, L. Ravi and R. Tallam, "Application of Active Gate Driver in Variable Frequency Drives," *2018 IEEE Energy Conversion Congress and Exposition (ECCE)*, Portland, OR, 2018, pp. 1796-1799.

[17] S. Wang, Y. Y. Maillet, F. Wang, D. Boroyevich and R. Burgos, "Investigation of Hybrid EMI Filters for Common-Mode EMI Suppression in a Motor Drive System," in *IEEE Transactions on Power Electronics*, vol. 25, no. 4, pp. 1034-1045, April 2010.

[18] D. O. Boillat, F. Krismer and J. W. Kolar, "EMI Filter Volume Minimization of a Three-Phase, Three-Level T-Type PWM Converter System," in IEEE Transactions on Power Electronics, vol. 32, no. 4, pp. 2473-2480, April 2017.

[19] A. Singh, A. Mallik and A. Khaligh, "A Comprehensive Design and Optimization of the DM EMI Filter in a Boost PFC Converter," in *IEEE Transactions on Industry Applications*, vol. 54, no. 3, pp. 2023-2031, May-June 2018.

[20] M. Antivachis, P. S. Niklaus, D. Bortis and J. W. Kolar, "Input/output EMI filter design for three-phase ultra-high speed motor drive gan inverter stage," in *CPSS Transactions on Power Electronics and Applications*, vol. 6, no. 1, pp. 74-92, March 2021.

[21] J. Biela, A. Wirthmueller, R. Waespe, M. L. Heldwein, K. Raggl, and J. W. Kolar, "Passive and active hybrid integrated emi filters," *IEEE Transactions on Power Electronics*, vol. 24, no. 5, pp. 1340–1349, May 2009.

[22] L. LaWhite and M. F. Schlecht, "Design of active ripple filters for power circuits operating in the 1-10 MHz range," *IEEE Trans. Power Electron.*, vol. 3, no. 3, pp. 310-317, Jul. 1988.

[23] T. Farkas, and M. F. Schlecht, "Viability of active EMI filters for utility applications," *IEEE Trans. Power Electron.*, vol. 9, no. 3, pp. 328-337, May 1994.

[24] C. Mei, J. C. Balda and W. P. Waite, "Cancellation of common-mode Voltages for induction motor drives using active method," *IEEE Transactions on Energy Conversion*, vol. 21, no. 2, pp. 380-386, June 2006.

[25] R. Goswami and S. Wang, "Modeling and Stability Analysis of Active Differential-Mode EMI Filters for AC/DC Power Converters," *IEEE Transactions on Power Electronics*, vol. 33, no. 12, pp. 10277-10291, Dec. 2018.

[26] M. L. Heldwein, H. Ertl, J. Biela and J. W. Kolar, "Implementation of a Transformerless Common-Mode Active Filter for Offline Converter Systems," *IEEE Transactions on Industrial Electronics*, vol. 57, no. 5, pp. 1772-1786, May 2010.

[27] W. Chen, X. Yang, J. Xue and F. Wang, "A Novel Filter Topology With Active Motor CM Impedance Regulator in PWM ASD System," *IEEE Transactions on Industrial Electronics*, vol. 61, no. 12, pp. 6938-6946, Dec. 2014.

[28] Y. Zhang, Q. Li and D. Jiang, "A Motor CM Impedance Based Transformerless Active EMI Filter for DC-Side Common-Mode EMI Suppression in Motor Drive System," *IEEE Transactions on Power Electronics*, vol. 35, no. 10, pp. 10238-10248, Oct. 2020.

[29] D. Shin, S. Jeong, and J. Kim, "Quantified Design Guidelines of Compact Transformerless Active EMI Filter for Performance, Stability, and High Voltage Immunity," *IEEE Trans. Power Electron.*, October 2017.

[30] Y. -. Son and Seung-Ki Sul, "A new active common-mode EMI filter for PWM inverter," *IEEE Transactions on Power Electronics*, vol. 18, no. 6, pp. 1309-1314, Nov. 2003.

[31] M. C. Di Piazza, A. Ragusa and G. Vitale, "An Optimized Feedback Common Mode Active Filter for Vehicular Induction Motor Drives," *IEEE Transactions on Power Electronics*, vol. 26, no. 11, pp. 3153-3162, Nov. 2011.

[32] D. Hamza, M. Qiu and P. K. Jain, "Application and Stability Analysis of a Novel Digital Active EMI Filter Used in a Grid-Tied PV Microinverter Module," *IEEE Transactions on Power Electronics*, vol. 28, no. 6, pp. 2867-2874, June 2013.

[33] J. Ji, W. Chen, X. Yang and J. Lu, "Delay and Decoupling Analysis of a Digital Active EMI Filter Used in Arc Welding Inverter," *IEEE Transactions on Power Electronics*, vol. 33, no. 8, pp. 6710-6722, Aug. 2018.

[34] H. Peng, B. Narayanasamy, A. I. Emon, Z. Yuan, R. Zhang and F. Luo, "Selective Digital Active EMI filtering using Resonant Controller," *2020 IEEE International Symposium on Electromagnetic Compatibility & Signal/Power Integrity (EMCSI)*, Reno, NV, USA, 2020, pp. 632-639.

[35] S. Wang, P. Kong and F. C. Lee, "Common Mode Noise Reduction for Boost Converters Using General Balance Technique," *IEEE Transactions on Power Electronics*, vol. 22, no. 4, pp. 1410-1416, July 2007.

[36] D. Dong, X. Zhang, F. Luo, D. Boroyevich, and P. Mattavelli, "Common-mode EMI noise reduction for grid-interface converter in low-voltage DC distribution system," *2012 IEEE Applied Power Electronics Conference and Exposition (APEC)*, Orlando, FL, 2012, pp. 451-457.

[37] Z. Zhang, W. Chen, A. M. Bazzi, S. Ramsay, J. Czapor, J. Aslanidis, "A new active EMI filter with virtual impedance enhancement," *2018 IEEE Applied Power Electronics Conference and Exposition (APEC)*, pp. 2393-2397, 2018.

[38] R. Goswami and S. Wang, "Investigation and Modeling of Combined Feedforward and Feedback Control Schemes to Improve the Performance of Differential Mode Active EMI Filters in AC–DC Power Converters," in *IEEE Transactions on Industrial Electronics*, vol. 66, no. 8, pp. 6538-6548, Aug. 2019.

[39] Y. Zhang and D. Jiang, "An Active EMI Filter in Grounding Circuit for DC Side CM EMI Suppression in Motor Drive System," in *IEEE Transactions on Power Electronics*, doi: 10.1109/TPEL.2021.3110144.

[40] S. Dey, A. Mallik and S. Mishra, "A Mathematical Design Approach to Volumetric Optimization of EMI Filter and Modeling of CM Noise Sources in a Three-Phase PFC," in *IEEE Transactions on Power Electronics*, vol. 37, no. 1, pp. 462-472, Jan. 2022.

[41] H. Li, Y. Ding, C. Zhang, Z. Yang, Z. Yang and B. Zhang, "A Compact EMI Filter Design by Reducing the Common-Mode Inductance With Chaotic PWM Technique," in *IEEE Transactions on Power Electronics*, vol. 37, no. 1, pp. 473-484, Jan. 2022.

[42] L. Middelstaedt, B. Strauss, A. Chupryn and A. Lindemann, "Investigation of the Root Causes of Electromagnetic Noise of an Interleaved DC–DC Converter With GaN or Si Transistors and Corresponding Optimization Strategies," in *IEEE Journal of Emerging and Selected Topics in Power Electronics*, vol. 8, no. 3, pp. 2759-2774, Sept. 2020.

[43] G. Giglia, G. Ala, M. C. Di Piazza, G. C. Giaconia, M. Luna, G. Vitale, P. Zanchetta, "Automatic EMI Filter Design for Power Electronic Converters Oriented to High Power Density", in *Electronics*. 2018; 7(1):9. https://doi.org/10.3390/electronics7010009.

[44] F. Viani, F. Robol, M. Salucci and R. Azaro, "Automatic EMI Filter Design Through Particle Swarm Optimization," in *IEEE Transactions on Electromagnetic Compatibility*, vol. 59, no. 4, pp. 1079-1094, Aug. 2017.

[45] G. Ala, G. C. Giaconia, G. Giglia, M. C. Di Piazza and G. Vitale, "Design and Performance Evaluation of a High Power-Density EMI Filter for PWM Inverter-Fed Induction-Motor Drives," in *IEEE Transactions on Industry Applications*, vol. 52, no. 3, pp. 2397-2404, May-June 2016.

[46] D. Shin et al., "Analysis and Design Guide of Active EMI Filter in a Compact Package for Reduction of Common-Mode Conducted Emissions," in *IEEE Transactions on Electromagnetic Compatibility*, vol. 57, no. 4, pp. 660-671, Aug. 2015.

[47] K. Zhang, K. -W. Wang and H. S. -H. Chung, "High-Attenuation Wideband Active Common-Mode EMI Filter Section," in *IEEE Transactions on Power Electronics*, vol. 37, no. 5, pp. 5479-5490, May 2022.

[48] D. Shin, S. Jeong, Y. Baek, C. Park, G. Park, and J. Kim, "A balanced feedforward current-sense current-compensation active EMI filter for common-mode noise reduction," *IEEE Trans. Electromagn. Compat.*, vol. 62, no. 2, pp. 386–397, Apr. 2020.

[49] R. Goswami, S. Wang, E. Solodovnik and K. J. Karimi, "Differential Mode Active EMI Filter Design for a Boost Power Factor Correction AC/DC Converter," in *IEEE Journal of Emerging and Selected Topics in Power Electronics*, vol. 7, no. 1, pp. 576-590, March 2019.

[50] C. Firek, "Active filters control EMI, save PCB space, and enhance airflow," PICOR Semiconductor Power Solutions, Tech. Article, Jun. 2004.